Bioresource Technology 442 (2026) 133707

Contents lists available at ScienceDirect

Bioresource Technology

journal homepage: www.elsevier.com/locate/biortech

# $S^0$ powder as biofilm carrier and electron donor enhances autotrophic nitrogen removal in sulfur-driven partial denitrification coupled with anammox

Sen Wang [a,b], Ben Dai [a,b,*], Zhenyu Wang [a,b], Shaobo Yang [a,b], Siqing Xia [a,b,*], Bruce E. Rittmann [c]

[a] State Key Laboratory of Pollution Control and Resource Reuse, College of Environmental Science and Engineering, Tongji University, Shanghai 200092, China
[b] Shanghai Institute of Pollution Control and Ecological Security, Shanghai 200092, China
[c] Biodesign Swette Center for Environmental Biotechnology, Arizona State University, Tempe, AZ 85287-5701, United States of America

## HIGHLIGHTS

- The $S^0$PDA process was established by integrating $S^0$ powders with anammox granules.
- Efficiency of total-nitrogen removal reached 92 %, with anammox contributing to 71 %.
- Microgranules promoted electron transfer between SOB and anammox bacteria.
- Autotrophic N—S cycle was achieved between suspended solids and anammox granules.
- Metagenomic analysis revealed unique functional genes in different spatial *niches*.

## GRAPHICAL ABSTRACT

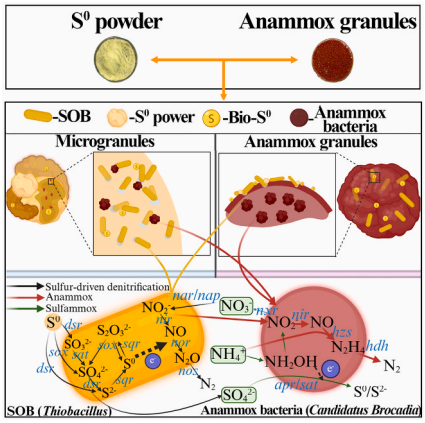


## ARTICLE INFO

*Keywords:*
Sulfur autotrophic denitrification
Microgranules
Metabolic pathway
Microbial niche
Metagenomic analysis

## ABSTRACT

Sulfur-driven partial denitrification coupled with anammox (SPD/A) has been proposed as an innovative strategy for nitrogen removal from wastewater. This study proposes a novel strategy that integrates 20-μm $S^0$ powders with anammox granules to establish $S^0$-driven partial denitrification coupled with anammox (i.e., $S^0$PD/A) for the simultaneous removal of $NH_4^+$ and $NO_3^-$ from wastewater. When the influent concentrations of $NH_4^+$ and $NO_3^-$ were maintained at 31 and 52 mg-N/L, respectively, the efficiency of total-nitrogen removal reached 92 %, with anammox, $S^0$-driven denitrification, and sulfammox accounting for 71 %, 27.4 %, and 1.6 %, respectively. Microbial community analysis revealed that anammox bacteria and sulfur-oxidizing bacteria were dominant functional genera involved in the $S^0$PD/A. Anammox bacteria were enriched in anammox granules, and sulfur-oxidizing bacteria were enriched in microgranules of $S^0$ powders and *Candidatus Brocadia*. These findings

* Corresponding authors at: Tongji University, 1239 Siping Road, Shanghai 200092, China.
*E-mail addresses:* daiben@tongji.edu.cn (B. Dai), siqingxia@tongji.edu.cn (S. Xia).

https://doi.org/10.1016/j.biortech.2025.133707
Received 10 August 2025; Received in revised form 13 October 2025; Accepted 24 November 2025
Available online 25 November 2025

highlight distinct microbial *niche* differentiation, elucidate nitrogen-sulfur metabolic interactions, and offer insights into an autotrophic process for total-nitrogen removal.

## 1. Introduction

Anaerobic ammonium oxidation (anammox) has emerged as a promising technology for nitrogen removal in wastewater treatment due to its better energy efficiency, lower sludge production, and elimination of demand for organic carbon compared to conventional biological removal of total-nitrogen (Jimenez et al., 2015). In anammox, ammonium ($NH_4^+$) and nitrite ($NO_2^-$) are converted into dinitrogen ($N_2$) by anammox bacteria in anoxic conditions (Strous et al., 1999). Large-scale application of anammox has been constrained by the challenge of maintaining a stable $NO_2^-$ supply achieved by partial oxidation of incoming $NH_4^+$ to $NO_2^-$ (Zhen et al., 2024). An alternative is heterotrophic partial denitrification (PD), which adds an organic electron donor to reduce $NO_3^-$ to $NO_2^-$ (Zhang et al., 2021). However, current PD systems require an external electron donor, which increases operational costs and $CO_2$ emissions, and PD may lead to secondary pollution due to discharge of residual organics (Du et al., 2020; Zhang et al., 2019). Additionally, the significantly faster specific growth rate of heterotrophic bacteria (e.g., 0.23 $h^{-1}$), compared to anammox bacteria (0.0075–0.014/h), may lead to overgrowth of heterotrophic bacteria that suppresses anammox bacteria activity and compromises nitrogen removal (Cao et al., 2021; Lotti et al., 2015).

The limitations of PD may be overcome by sulfur-driven partial denitrification (SPD), mediated by sulfur-oxidizing bacteria (SOB) coupled with anammox (Gu et al., 2024). In SPD, reduced sulfur compounds, such as sulfide ($S^{2-}$) and thiosulfate ($S_2O_3^{2-}$), serve as electron donors for SOB to reduce $NO_3^-$ into $NO_2^-$ (Wang et al., 2023). Compared to heterotrophic bacteria, SOB have lower specific growth rates (0.04–0.27 $h^{-1}$) and stronger preference for $NO_3^-$ reduction over $NO_2^-$ reduction (Zhou et al., 2011), making SPD more compatible with anammox (Kosgey et al., 2021). SPD coupled with anammox (i.e., SPD/A) eliminates the need for adding an organic electron donor, and it reduces sludge production, and mitigates $CO_2$ emissions. Additionally, the denitrification process is controlled at the $NO_2^-$ stage, which helps reduce $N_2O$ emissions (Gu et al., 2024; Hu et al., 2020).

While SPD/A has significant potential, concerns remain regarding its operational stability and cost-effectiveness (Deng et al., 2022). Both aspects should be benefited by using elemental sulfur ($S^0$) as the electron donor for denitrification, since $S^0$ is readily available from natural sulfur mines or industrial by-products (Li et al., 2023). Compared to $S_2O_3^{2-}$ and $S^{2-}$, $S^0$ also is less toxic and less expensive (Zeng et al., 2021). Being a solid, $S^0$ can act as a substratum for SOB attachment, which may be compatible with anammox granule (Wang et al., 2024b).

Previous studies have shown that smaller $S^0$ particles increase denitrification kinetics; thus, $S^0$ powders may achieve better nitrogen removal when coupled with anammox than larger $S^0$ particle (Li et al., 2023). Meanwhile, as $S^0$ serves as a carrier in the $S^0$PD/A system, using smaller $S^0$ powder to increase the specific surface area can accelerate microbial aggregation and biofilm formation (Wang et al., 2024a). Overall, $S^0$ powders can promote formation of microgranules of $S^0$ and microorganisms, which should improve the retention of SOB biomass and enhance nitrogen-removal efficiency (Li et al., 2023; Liang et al., 2022; Wang et al., 2023). Up to now, research on $S^0$PD/A focused on $S^0$ particles, not $S^0$ powders. Additionally, previous studies have revealed the occurrence of sulfammox in $S^0$PD/A (Yin et al., 2025; Zhu et al., 2022). In sulfammox, $NH_4^+$ is oxidized to $N_2$, while sulfate ($SO_4^{2-}$), which is produced by SOB oxidation of $S^0$, is reduced to $S^0$ and utilized again as an electron donor. Therefore, since sulfammox should enhance N—S metabolic interactions, it is crucial to investigate interactions among anammox, $S^0$-driven denitrification ($S^0$D), and sulfammox in $S^0$PD/A using $S^0$ powders as the electron donor.

Here, this study explores the feasibility of using $S^0$ powders as an electron donor for an $S^0$PD/A system treating wastewater containing $NH_4^+$ and $NO_3^-$ (such as the effluents of mine, mill, and fertilizer factory (Deng et al., 2019b)). A sequencing batch reactor (SBR) was established and operated continuously for 170 days to evaluate the nitrogen-removal efficiency and stability of $S^0$PD/A. Physical characteristics of biomass were analyzed, and denitrification pathways were explored through batch experiments. Fluorescence in situ hybridization (FISH), high-throughput 16S rDNA amplicon sequencing, and metagenomic sequencing were employed to reveal microbial community succession, spatial *niches* of bacteria, and interactions between SOB and anammox bacteria.

## 2. Materials and methods

### 2.1. Reactor set-up and operation

A novel $S^0$PD/A system was developed in a laboratory-scale SBR reactor with working volume of 3.0 L and a volume exchange ratio of 50 %. It was equipped with a mechanical stirrer (150 rpm) for mixing. The reactor temperature was maintained at 35 ± 1℃ by recirculating water from a water bath to the inner and outer walls of the SBR. The reactor was operated with three cycles per day, with each cycle lasting 8 h: 7 h of reaction time, 0.5 h of settling time, and 0.5 h of idle time. The SBR reactor was operated for 170 days that were divided into 2 phases: Phase 1 (0–70 days) focused on $S^0$-driven partial denitrification, while Phase 2 (71–170 days) was dedicated to $S^0$PD/A. To provide electron donor and carrier for the SOB, 20 g of $S^0$ powders were initially added, followed by a daily addition of 0.5 g according to the $NO_3^-$-N loading (Chen et al., 2018). Table S1 shows the operational conditions and Fig. S1 shows the physical characteristics of $S^0$ powder.

To begin Phase 1, the SBR was seeded with secondary-sedimentation sludge obtained from a wastewater treatment plant in Shanghai. The seeding sludge did not contain significant abundances of SOB or anammox bacteria, and the initial concentrations of mixed liquor suspended solids (MLSS) and mixed liquor volatile suspended solids (MLVSS) were 4.6 g/L and 3.7 g/L, respectively. In Phase 2, 500 mL of anammox granules were introduced into the SBR to initiate $S^0$PD/A. The anammox granules were obtained from a laboratory-scale anammox SBR that had been operating stably with $NO_2^-$ and $NH_4^+$ as substrates. The MLSS and MLVSS concentrations of the anammox sludge were 3.3 g/L and 2.9 g/L, respectively.

To simulate the water quality of wastewater containing $NO_3^-$ and $NH_4^+$, synthetic wastewater was prepared by dissolving predefined amounts of $NH_4Cl$ and $NaNO_3$ in tap water, with the concentrations varying according to different operational phases. Additionally, mineral medium contained $KH_2PO_4$ (27.2 mg/L), $MgCl_2{\cdot}6H_2O$ (247.4 mg/L), $CaCl_2{\cdot}2H_2O$ (180 mg/L), $KHCO_3$ (500 mg/L), and 1 mL/L of trace element solutions A and B (Zhang et al., 2022). The compositions of the trace element solutions are provided in Text S1.

### 2.2. Analytical methods

Water samples were collected and filtered through 0.22-μm membrane filters (Titan, Shanghai, China). The MLSS, MLVSS, sludge settling velocity (SV), sludge volume index (SVI), and concentrations of $NH_4^+$, $NO_2^-$, and $NO_3^-$ were measured according to standard methods (APHA, 1998). The concentration of $SO_4^{2-}$ was measured using ion chromatography (Thermo Fisher, USA).

The morphology and element distribution of $S^0$ powders and solids were analyzed by scanning electron microscope (SEM, Zeiss Gemini 300,

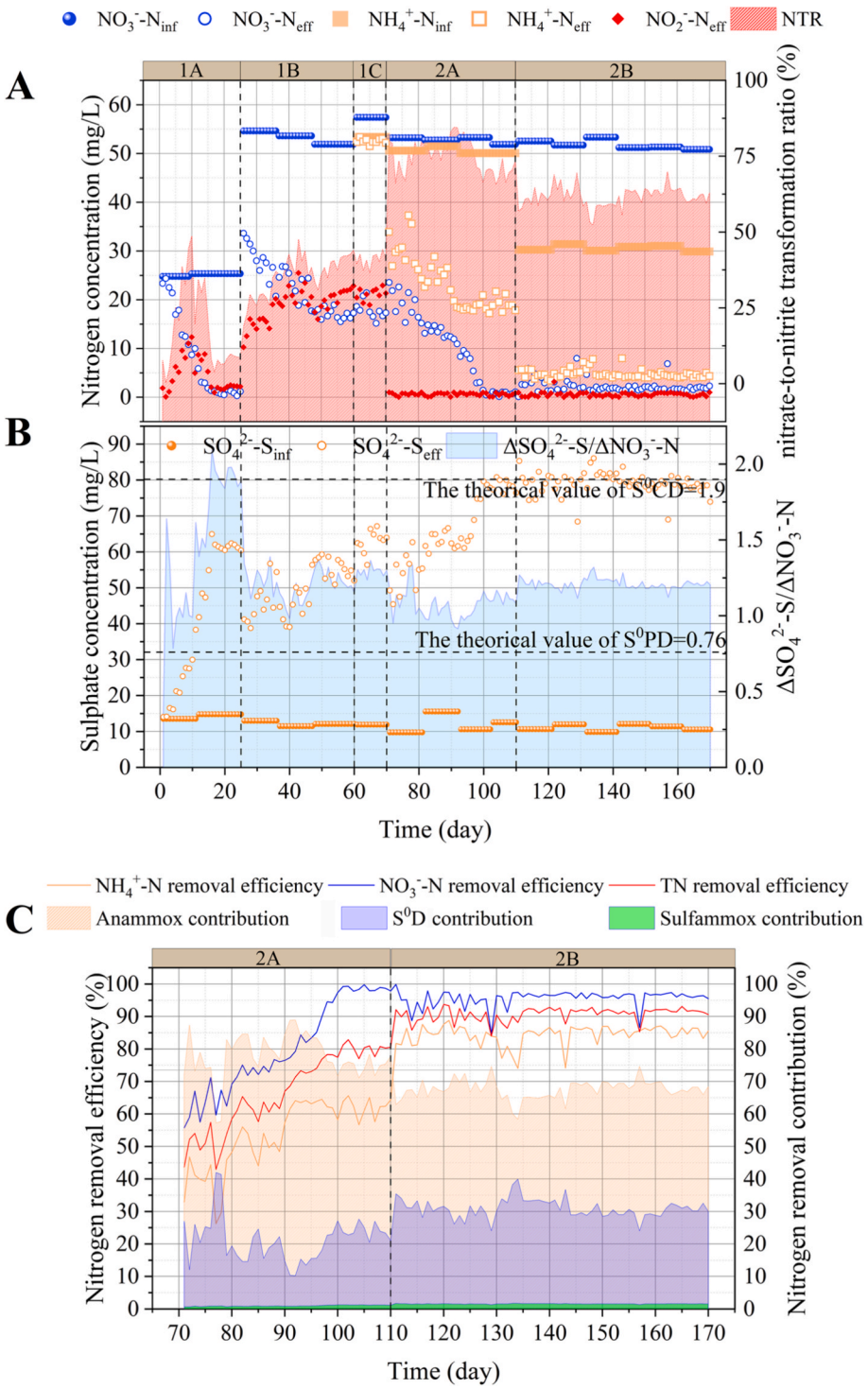


**Fig. 1.** Overall performance of the $S^0$PD/A reactor: influent and effluent nitrogen concentrations and the $NO_3^-$-to-$NO_2^-$ transformation ratio (NTR) (A); influent and effluent $SO_4^{2-}$-S concentrations and the $\Delta SO_4^{2-}$-S/$\Delta NO_3^-$-N (B); efficiency of $NH_4^+$-N, $NO_3^-$-N, and TN removal and contribution of anammox, $S^0$D, and sulfammox to total-nitrogen removal in Phase 2 (C).

Germany) and energy dispersive spectroscopy (EDS, Oxford Xplore, Britain). Functional groups of biomass samples were analyzed using the Fourier Transform Infrared Spectroscopy (FTIR, Thermo Fisher, USA). X-Ray Photoelectron Spectroscopy (XPS, Thermo Scientific, USA) and X-Ray Diffraction (XRD, Rigaku, Japan) were used to identify various elemental compositions and crystalline structure. Fluorescence *in situ* hybridization (FISH) was employed to examine the spatial distribution of different bacteria within suspended biomass and anammox granules. The soluble microbial products (SMP), loosely bound EPS (LB-EPS), and tightly bound EPS (TB-EPS) were collected and filtered through a 0.45-μm filter membrane for analysis (Yin et al., 2025). Protein (PN) and polysaccharides (PS) in SMP and EPS were determined based on the Lowry-Folin method and phenol–sulfuric acid method (Wang et al., 2024a). Three-dimensional excitation-emission matrix (3D-EEM) spectra of TB-EPS were obtained using a fluorescence photometer. More details about analytical methods are in Text S2, calculations are in Text

S4 and Text S5.

### 2.3. Batch experiments

Three sets of batch experiments were conducted to elucidate the nitrogen-removal pathways of $S^0$PDA, and the experimental conditions are summarized in Table S2. During the end of phase 2B of the reactor, the suspended solids, anammox granules, and a mixture of the two were collected separately from the bioreactor and washed three times with 0.1-M phosphate-buffered saline (PBS). Then, the inoculum was mixed with 80 mL of simulated wastewater and supplemented with 1 g of $S^0$ powders. The mixture was placed into 100-mL serum bottles for batch experiments. To establish an anoxic environment, nitrogen gas ($N_2$) was purged into the bottles for 10 min to remove dissolved oxygen (DO). All experiments were performed in a shaker at 150 rpm and 35 ± 1 °C. During the experiments, water samples were collected at predetermined time intervals, filtered through 0.22-μm filter membranes, and stored at 4 °C for further analysis.

### 2.4. Microbial community analysis

For 16S rDNA amplification and sequencing, suspended solids were collected at the end of Phase 1A and Phase 2B, and anammox granules were collected at the end of Phase 2A and Phase 2B. DNA extraction was conducted using the DNeasy PowerBiofilm Kit (50) (QIAGEN, Germany). The V3-V4 region of bacterial 16S rDNA gene was amplified with the forward primer 338F (5′-ACTCCTACGGGAGGCAGCAG-3′) and reverse primer 806R (5′-GGACTACNNGGGTATCTAAT-3′). 16S rDNA gene amplification and sequencing were performed on Illumina Next-seq2000 platform (Illumina, San Diego, USA) according to the standard protocols by Majorbio Bio-Pharm Technology Co. Ltd. (Shanghai, China). Principal co-ordinates analysis (PCoA) was employed to explore differences in the microbial community over long-term operation (Wang et al., 2024b). For metagenomic sequencing, paired-end sequencing was performed on Illumina NovaSeq™ X Plus (Illumina Inc., San Diego, CA, USA) at Majorbio Bio-Pharm Technology Co., Ltd. (Shanghai, China) using NovaSeq X Series 25B Reagent Kit. Detailed information is in Text S3. Raw sequencing data are available from the NCBI database with accession number PRJNA1266653.

## 3. Results and discussion

### 3.1. Long-term nitrogen-removal performance of the SBR reactor

Phase 1 was divided into three sub-phases: 1A (Days 0–25), 1B (Days 26–60), and 1C (Days 61–70). Performance results are presented in Fig. 1. Phase 1A initiated $S^0$-driven denitrification. After 25 days of acclimation, the effluent $NO_3^-$ and $NO_2^-$ concentrations decreased to 1 mg-N/L and 2 mg-N/L, respectively. In Phase 1B, the influent $NO_3^-$ concentration was increased to 53.3 ± 1.2 mg-N/L with effluent $NO_2^-$ concentration peaking at 25.5 mg-N/L (Fig. 1A). The $NO_3^-$-to-$NO_2^-$ transformation ratio (NTR) (calculation is in Text S5) reached 48 %, indicating successful establishment of $S^0$PD (Deng et al., 2019b). In Phase 1C, 53 mg-N/L of $NH_4^+$ was added and the $NH_4^+$-removal efficiency remained below 4 %, meaning that the reactor was unable to effectively remove $NH_4^+$ with $S^0$PD alone.

The mass ratio of produced $SO_4^{2-}$-S to consumed $NO_3^-$-N ($\Delta SO_4^{2-}$-S/$\Delta NO_3^-$-N) helps distinguish the relative contributions of $S^0$-driven complete denitrification ($S^0$CD) and $S^0$PD. In the $S^0$PD pathway, $NO_3^-$ is partially reduced to $NO_2^-$, which is subsequently removed via anammox. In the $S^0$CD pathway, $NO_2^-$ is further reduced to $N_2$, leading to greater $SO_4^{2-}$ production. Theoretically, the $\Delta SO_4^{2-}$-S/$\Delta NO_3^-$-N ratio is 1.9 mg-S/mg-N for $S^0$CD and 0.76 mg-S/mg-N for $S^0$PD, based on the stoichiometry in Text S4. At the beginning of Phase 1B, a sharp increase in influent $NO_3^-$ concentration led to incomplete $NO_3^-$ reduction by SOB, resulting in the accumulation of $NO_2^-$. The $\Delta SO_4^{2-}$-S/$\Delta NO_3^-$-N ratio declined from 1.93 mg-S/mg-N to 1.18 mg-S/mg-N, suggesting that $S^0$PD was the dominant pathway (Fig. 1B). $NO_2^-$ accumulation likely was due to higher enzymatic activity of SOB's nitrate reductase compared to its nitrite reductase (Deng et al., 2022). By the end of Phase 1C, this ratio gradually increased to 1.29 mg-S/mg-N, indicating that SOB began adapting to the elevated $NO_3^-$ levels so that the $S^0$CD contribution could increase. Since $S^0$CD typically dominates during long-term operation of $S^0$-driven denitrification systems (Chen et al., 2018), having $S^0$PD still predominate at the end of Phase 1C was optimal for the subsequent introduction of anammox bacteria in Phase 2.

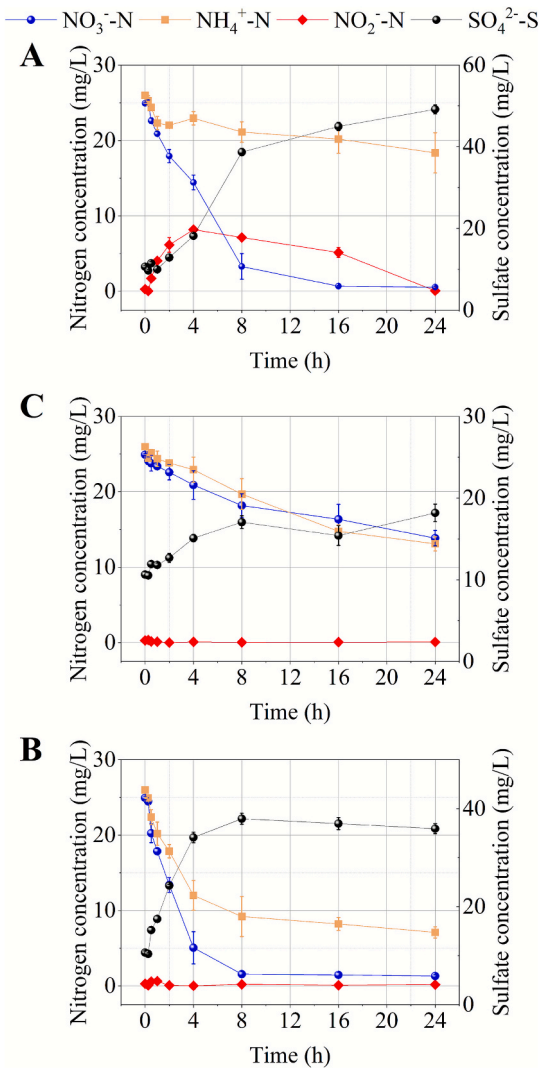


**Fig. 2.** Results of batch experiments with different biomass types: suspended solids (A); anammox granules (B); and the combined system (suspended solids and anammox granules) (C).

Phase 2 was divided into two sub-phases: Phase 2A (startup, days 71–110) and Phase 2B (stable operation, days 111–170). To establish $S^0$PD/A, enriched anammox granules were introduced into the SBR reactor on day 71. In Phase 2A, the influent concentrations of $NO_3^-$ and $NH_4^+$ were maintained at 52.8 ± 0.5 mg-N/L and 50.6 ± 0.6 mg-N/L, respectively. Following inoculation of the anammox granules, the effluent $NH_4^+$ concentration dropped to 33 mg-N/L on day 71 and further decreased to 19 mg-N/L by the end of Phase 2A, which corresponded to a $NH_4^+$-removal efficiency of 62 %. Simultaneously, the $NO_3^-$ concentration also declined to 1 mg-N/L, with a $NO_3^-$-removal efficiency of 99 % (Fig. 1C). From day 92 to the end of Phase 2A, the $\Delta SO_4^{2-}$-S/$\Delta NO_3^-$-N ratio increased from 0.91 mg-S/mg-N to 1.11 mg-S/mg-N, the NTR decreased from 85 % to 70 %, and $S^0$D's contribution to total-nitrogen

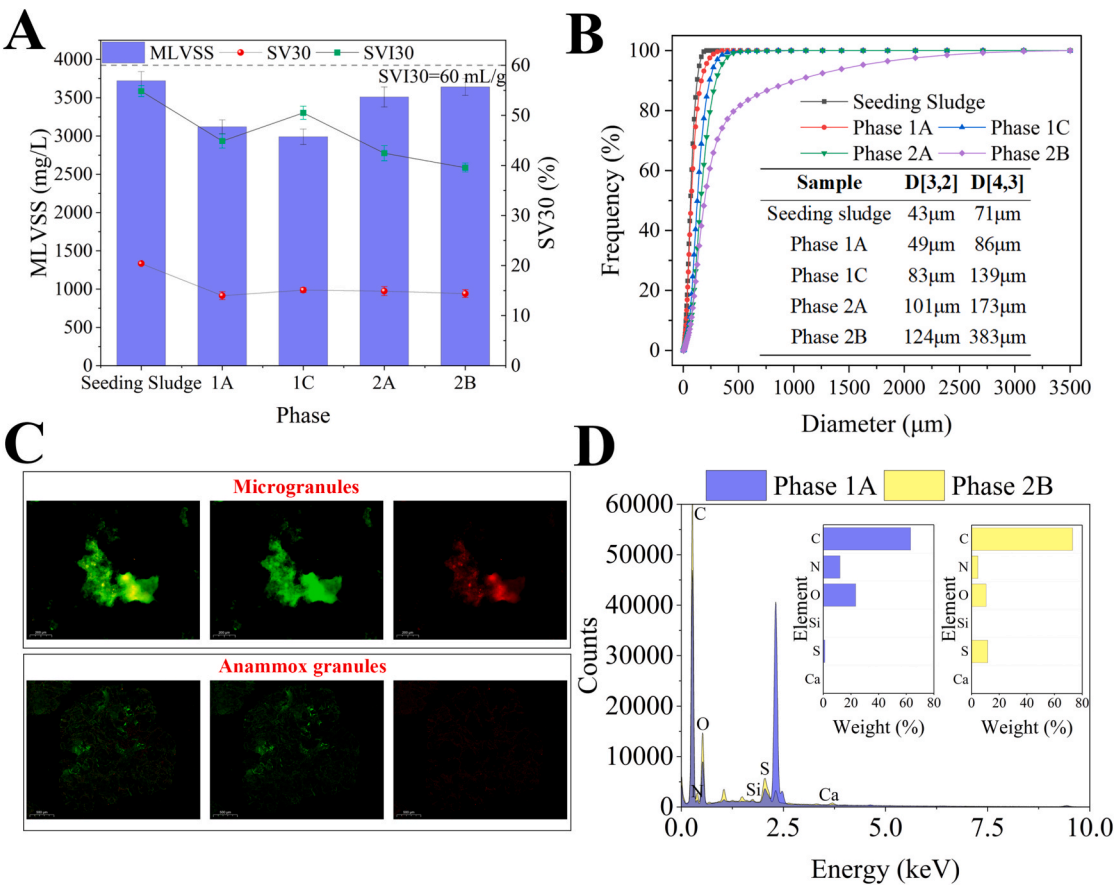


**Fig. 3.** Physical characterization of biomass: MLVSS, SV30, and SVI30 (A); cumulative graph of particle size (B); FISH analysis of microgranules and anammox granules (SOB labelled with 5′, 6-FAM green and anammox bacteria labelled with 5′, CY5 red) (C); and Elemental analysis (D).

removal correspondingly increased from 9 % to 22 %; thus, $NO_2^-$ reduction to $N_2$ occurred via $S^0$CD (Fig. 1C). The suboptimal $NH_4^+$-removal efficiency (62 %) can be attributed to SOB out-competing anammox bacteria for $NO_2^-$ due to a relatively low proportion of anammox granules compared to denitrifying sludge (Du et al., 2024).

During Phase 2B, the influent $NH_4^+$ concentration was lowered to 31 mg-N/L in order to lower residual $NH_4^+$ in the effluent, and a rapid decrease in effluent $NH_4^+$ concentration was observed: the effluent $NH_4^+$ and $NO_3^-$ concentrations stabilized at 4.4 mg-N/L and 1.9 mg-N/L, respectively. Meanwhile, sulfammox activity also was observed during Phase 2, with its contribution to total-nitrogen removal increasing from 1.2 % in Phase 2A to 1.6 % in Phase 2B. The mass-balance analysis in Text S5 confirmed that anammox had a contribution of 71 % to total-nitrogen removal in Phase 2B and was the dominant nitrogen-removal pathway. Compared to anammox contribution of 75 % in Phase 2A, this slight decrease was attributed to the reduced influent $NH_4^+$ concentration and the decreased activity of anammox bacteria caused by interspecies competition (Deng et al., 2019b). However, the total-nitrogen removal efficiency increased from 81 % in Phase 2A to 92 % in Phase 2B, indicating effective nitrogen-removal under the optimized influent conditions.

### 3.2. Metabolic pathways of $S^0$PD/A

Three sets of batch experiments were conducted to investigate nitrogen-removal pathways of suspended solids and anammox granules in the $S^0$PD/A process, with experiments design in Table S2 and results in Fig. 2. When only suspended solids were present, $NO_3^-$ decreased significantly, while $NO_2^-$ accumulated, with a slight decrease of $NH_4^+$ (Fig. 2A), suggesting that $S^0$PD dominated the suspended solids, while anammox activity was limited there. When only anammox granules were present, $SO_4^{2-}$ production and removal of $NO_3^-$ and $NH_4^+$ were observed (Fig. 2B). This can be attributed to SOB that attached to the surface of anammox granules and supplied $NO_2^-$ for anammox bacteria (Yin et al., 2025). Suspended solids and anammox granules were combined to simulate reactor conditions (Fig. 2C). After 8 h, a decline in $NH_4^+$ and $SO_4^{2-}$ concentrations suggested the occurrence of sulfammox. After 24 h, the removal efficiencies of $NO_3^-$ and $NH_4^+$ reached 94 % and 73 %, respectively. The contributions of anammox, $S^0$D, and sulfammox to total-nitrogen removal were 80 %, 16 %, and 4 %, respectively. Thus, anammox was the dominant nitrogen-removal pathway in the $S^0$PD/A process, with $S^0$D and sulfammox providing support.

### 3.3. Biomass characteristics

#### 3.3.1. Physical characterization of solids and spatial niches of bacteria

No biomass washout was observed during the entire operation and physical characterization of solids and spatial *niches* of bacteria are presented in Fig. 3. As shown in Fig. 3A, after the addition of $S^0$ powders, the MLVSS initially decreased due to the change in electron donor but subsequently increased and stabilized. The $SVI_{30}$, used to evaluate flocculent and compact characteristics of the biomass (Lu et al., 2023), decreased from 20.4 mL/g in the seeding sludge to 14.4 mL/g in Phase 2B, indicating excellent settling performance of the suspended solids. Fig. 3B presents the cumulative particle-size distributions for the suspended solids across different operational stages, where D[3,2] represents the Sauter mean diameter and D[4,3] represents the De Brouckere mean diameter. In the seeding sludge, D[3,2] and D[4,3] were 43 μm and 71 μm, respectively. Following addition of $S^0$ powders, the particle sizes increased significantly, with D[3,2] and D[4,3] reaching 124 μm

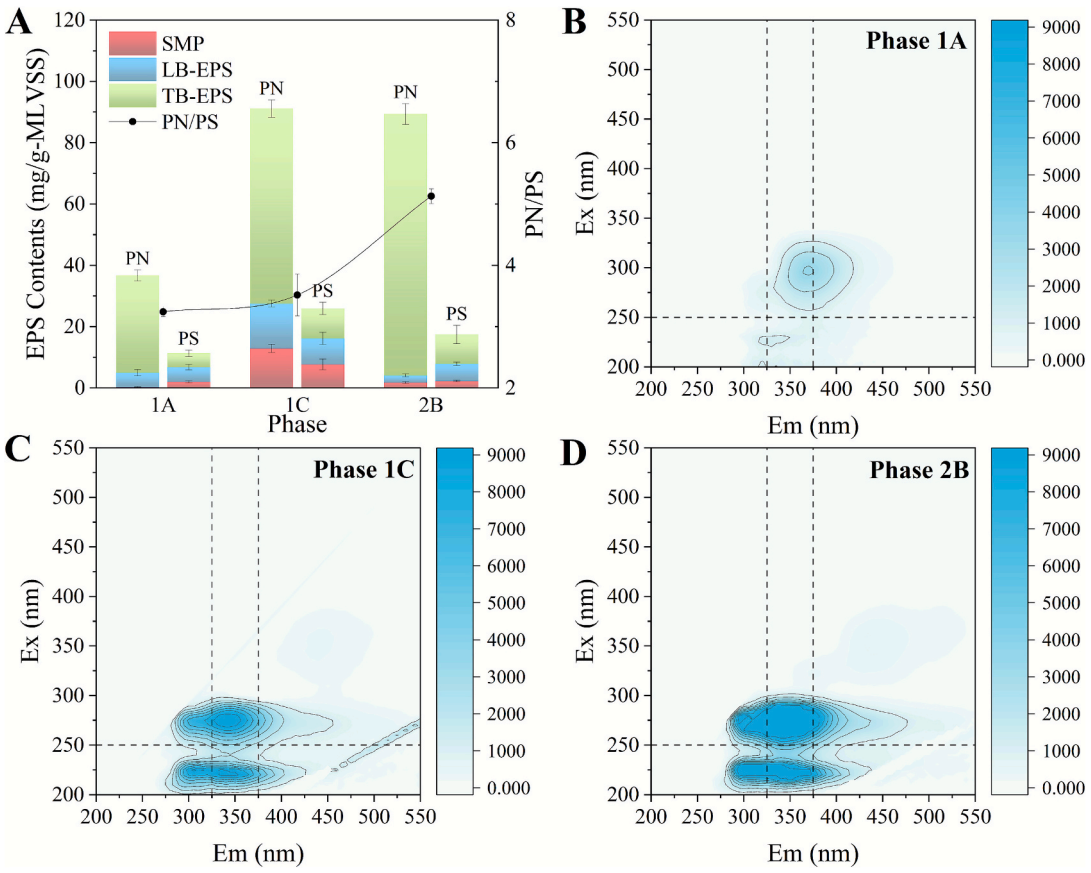


**Fig. 4.** SMP and EPS characteristics in phases 1A, 1C, and 2B: SMP, EPS, and PN/PS ratio (A); and EEM spectra of TB-EPS: (B-D).

and 383 μm, respectively, in Phase 2B. FTIR, XRD, and XPS analysis revealed enhanced hydrophobicity and amorphous structures of biomass after $S^0$ powders addition with results in Fig. S2. As a powdered carrier, $S^0$ powder enhanced biomass settling ability, improved biomass concentration, and promoted formation of microgranules (Wang et al., 2024a; Wang et al., 2021; Wu et al., 2022).

The surface morphology of biomass was examined by SEM, with results in Fig. S3. Although $S^0$ powders theoretically could serve as a core for anammox bacteria to aggerate (Xue et al., 2023), anammox granules with $S^0$ powders were not observed. Instead, $S^0$ powders were embedded within suspended solids, thereby forming microgranules. The spatial distribution of anammox bacteria and SOB in microgranules and anammox granules was investigated using FISH analysis, with results in Fig. 3C and detailed methods in Text S2. Anammox bacteria and SOB were evenly distributed in microgranules. In anammox granules, SOB was primarily located in porous structure on the surface of the granules. This porous structure and spatial distribution of microbial community may have promoted substrate exchange, electron transport, and microbial interactions (Wang et al., 2022; Xue et al., 2023). SEM combined with EDS analysis, shown in Fig. S3, reveals that the clustered crystalline structures observed on the surface of anammox granules were composed of $S^0$, consistent with a previous study of a SPD/A process (Jiang et al., 2025). These crystals were likely bio-$S^0$ (polysulfides produced by $S^0$ disproportionation or $S^0$ produced via sulfammox), which could enhance $S^0$ bioavailability and denitrification performance (Liu et al., 2025; Qian et al., 2021). EDS analysis, presented in Fig. 3D, show that the S content in suspended solids increased after the addition of $S^0$ powders, which may be attributed to the $S^0$ powders accumulating within microgranules.

### 3.3.2. SMP and EPS characterization

SMP and EPS, which play a crucial role in microbial aggregation and sludge granulation, were extracted to quantify PN and PS contents at different phases; results are in Fig. 4A (Wang et al., 2024a). The total EPS, which includes SMP, LB-EPS and TB-EPS, increased from 48 mg/g-MLVSS in Phase 1A to 107 mg/g-MLVSS in Phase 2B, indicating effective microgranule formation within the suspended solids. Among the three fractions, TB-EPS exhibited the highest content, increasing from 36 mg/g-MLVSS in Phase 1A to 95 mg/g-MLVSS in Phase 2B, suggesting that TB-EPS may play a more important role in microgranule formation. PN and PS concentrations increased over time, PN was higher than PS and most of PN was TB-EPS. From Phase 1A to Phase 2B, the PN in TB-EPS increased from 32 to 85 mg/g-MLVSS, and the PN/PS ratio rose from 3.3 to 5.1. A higher PN/PS ratio can enhance the hydrophobicity and stability of biomass (Campo et al., 2018). In addition, the PS in TB-EPS, which can act as a structural scaffold to enhance bacterial adhesion and biomass aggregation (Wang et al., 2020), increased over time.

3D-EEM fluorescence spectroscopy was employed to analyze the composition of TB-EPS in suspended solids, shown in Fig. 4B–D. The fluorescence regions in the spectra were identified based on established classification (Yin et al., 2015; Yu et al., 2023). Fluorescence intensity related to tyrosine-like (regions I/II) and tryptophan-like substances (region IV) increased, indicating that microorganisms secreted more protein-like compounds in response to $S^0$. Additionally, a fluorescence peak related to polysaccharide-like substances (region V) was detected in Phase 2B, but not in Phase 1A, which is consistent with the increased PS content observed in TB-EPS. Microgranules can facilitate interspecies electron transfer because tyrosine-like and humic acid-like substances can function as electron mediators (Yin et al., 2025).

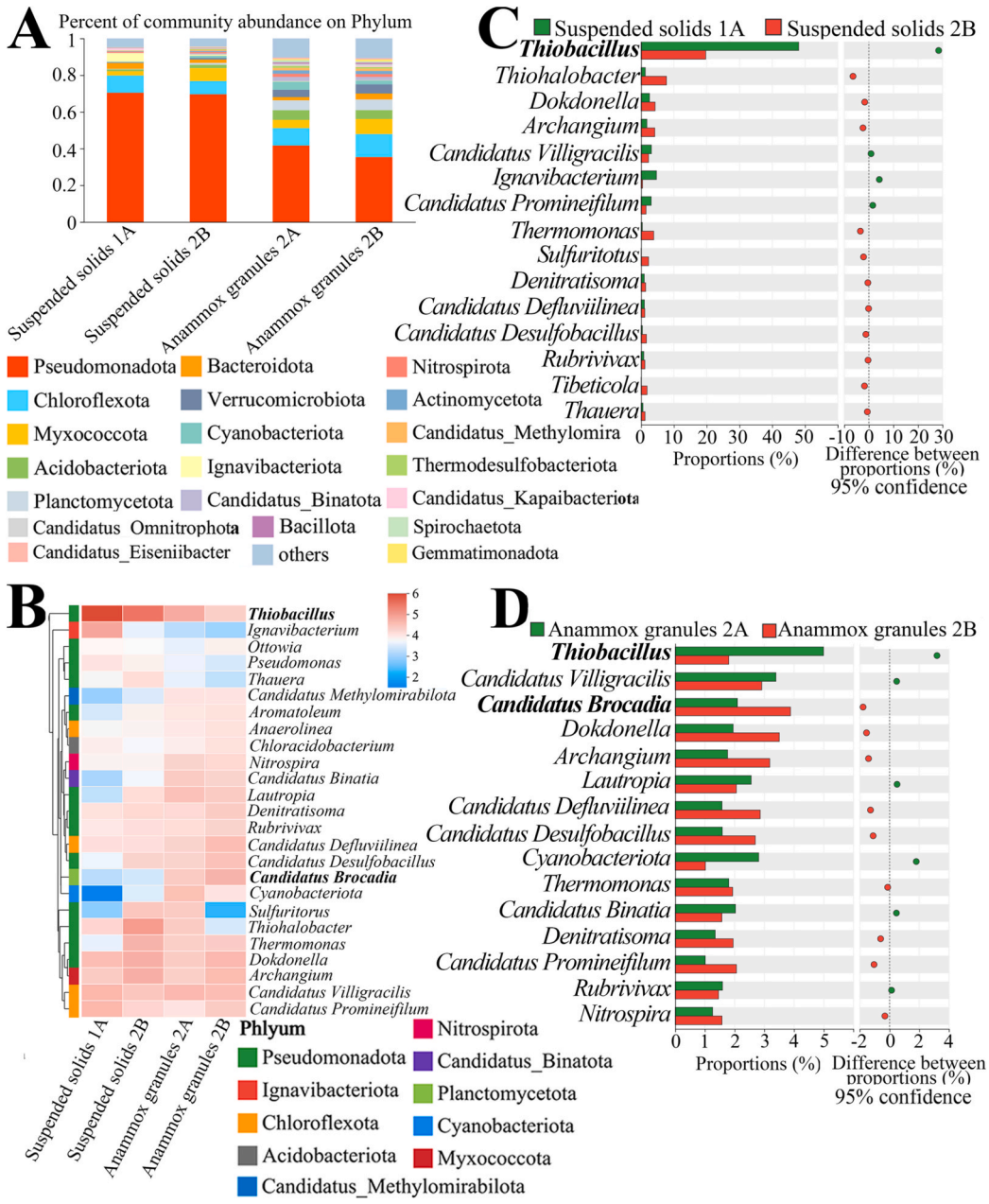


**Fig. 5.** Microbial community characteristics of the $S^0$PD/A system: changes in microbial community at the phylum level (A); heatmap at the genus level (B); microbial community characteristics of suspended solids (C); and microbial community characteristics of anammox granules (D).

### 3.4. Microbial analysis

#### 3.4.1. Microbial community succession of suspended biomass and anammox granules

As shown in Fig. 5A, the dominant microorganisms at the phylum level were *Pseudomonadota*, *Chloroflexota, Acidobacteriota*, *Planctomycetota*, and *Myxococcota*. The relative abundance of *Planctomycetota* (which include anammox bacteria) increased from 0.26 % to 1 % in suspended biomass and from 5.4 % to 5.8 % in anammox granules (Yin et al., 2025). *Chloroflexiota*, which can promote biofilm formation (Wang et al., 2024a), accounted for 7.21 % of the microbial community in suspended biomass in Phase 2B and might have played a role in microgranules formation.

The microbial community at the genus level is shown in Fig. 5B–D. *Thiobacillus*, a typical SOB (Deng et al., 2019a), was dominant in suspended biomass, but its relative abundance decreased from 48.1 % in Phase 1A to 19.7 % in Phase 2B (Fig. 5C). *Thiobacillus* also was detected in anammox granules with abundance decreasing from 5 % in Phase 1A to 1.8 % in Phase 2B, which helps explain the removal of $NO_3^-$ and $NH_4^+$ observed in batch experiment B because *Thiobacillus* could provide $NO_2^-$ for anammox granules (Fig. 5D). The decrease in the relative abundance of *Thiobacillus* may be attributed to the competitive utilization of $NO_2^-$ by anammox (Yin et al., 2025).

The relative abundance of *Thiohalobacter*, which can oxidize $S^0$ to $SO_4^{2-}$, increased from 1.3 % to 7.7 % in suspended biomass. In addition, heterotrophic denitrifying bacteria were detected in the suspended biomass, including *Thermomonas* (3.8 %) and *Denitratisoma* (2.3 %). These bacteria can reduce $NO_3^-$ using EPS or SMP as electron donors, and their relatively high abundance was related to the formation of microgranules.

*Candidatus Brocadia*, the only anammox bacterium detected in the reactor, increased from 0.16 % to 0.28 % in suspended biomass and from

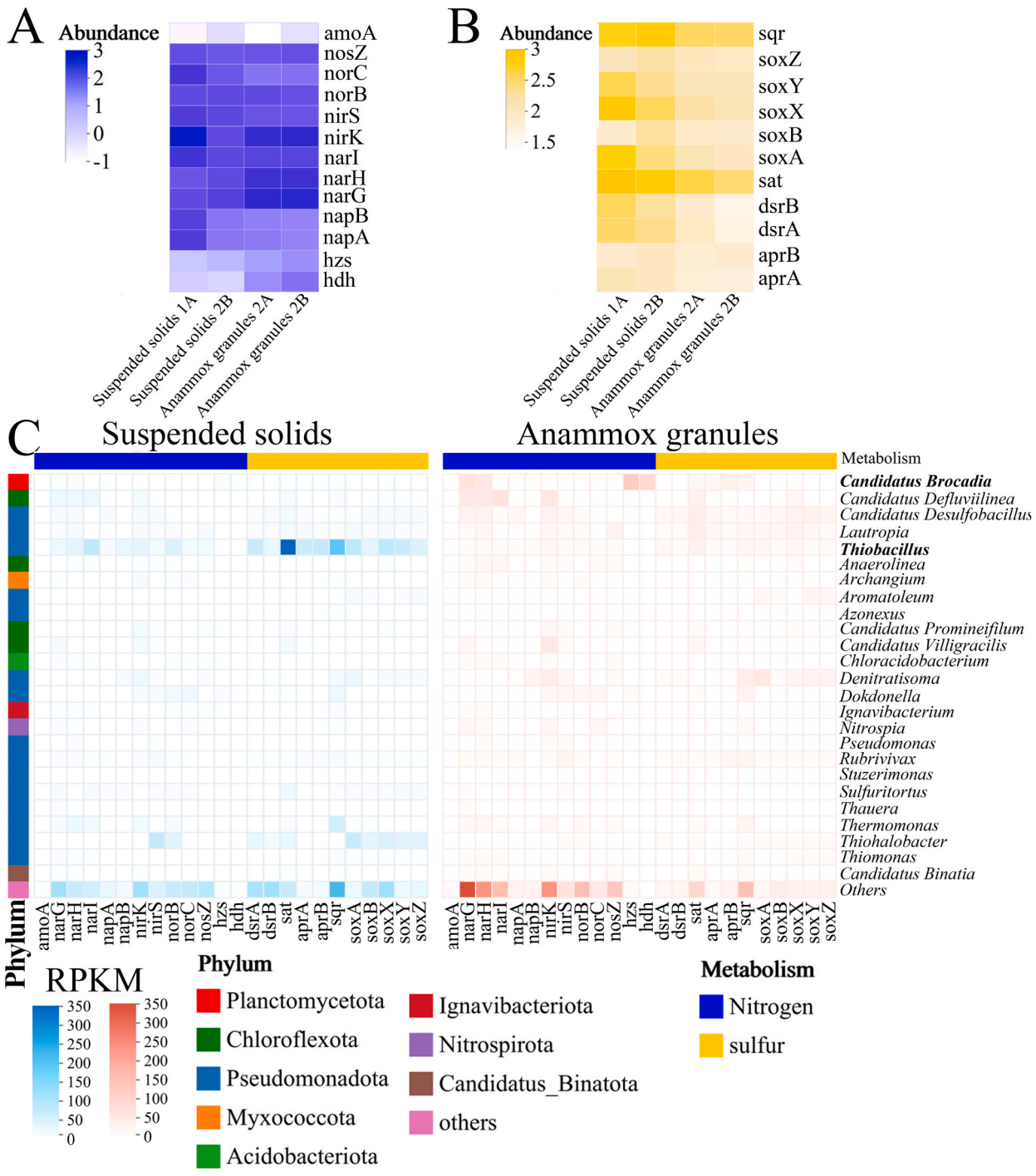


**Fig. 6.** Distribution of functional genes related to N—S metabolic interactions: genes related to nitrogen metabolic mechanism in different operation phases (A); genes related to sulfur metabolic mechanism in different operation phases (B); and taxonomic origins of the key genes in Phase 2B (C).

2.1 % to 3.9 % in anammox granules, which implies that the addition of $S^0$ powders to the $S^0$PD/A reactor promoted the growth of *anammox bacteria* (Yin et al., 2025). Additionally, PCoA analysis, which is shown in Fig. S4, reveals that microbial richness in the suspended biomass was much lower than in the anammox granules.

### 3.4.2. *Distribution of functional genes related to N—S metabolic interactions*

The results of metagenomic sequencing, conducted to investigate changes in functional genes related to N—S metabolic interactions, are summarized in Fig. 6. As shown in Fig. 6A, *N*-related genes were significantly different among the phases. The *hzs* gene (encoding hydrazine synthase) and the *hdh* gene (encoding hydrazine dehydrogenase), which are related to the central energy metabolism of anammox bacteria, increased from Phase 2A to Phase 2B in anammox granules; this means that the activity of anammox bacteria was well-maintained when the influent $NH_4^+$ concentration was lowered in Phase 2B. The taxonomic origins of the key genes in Phase 2B are shown in Fig. 6C. In anammox granules, the *hzs* and the *hdh* gene were primarily associated with *Candidatus Brocadia*. Notably, these genes also were detected in suspended biomass, supporting the fact that anammox activity could have occurred there, as well.

The denitrification process is catalyzed by $NO_3^-$ reductase, $NO_2^-$ reductase, NO reductase, and $N_2O$ reductase. In the suspended biomass, the *nar* gene (encoding $NO_3^-$ reductase), the *nap* gene (encoding $NO_3^-$ reductase), and the *nir* gene (encoding $NO_2^-$ reductase) were primarily attributed to *Thiobacillus* (Fig. 6C). The (*nar* + *nap*) to *nir* ratio, which is used to evaluate the capacity of $NO_2^-$ accumulation (Wang et al., 2024b), was 3.2 in the suspended biomass, which exceeds a threshold value of 3.1 to have *Thiobacillus* provide a sufficient supply of $NO_2^-$ for *Candidatus Brocadia*. Notably, functional gene *amoA* (encoding the enzyme for the first step of nitrification) was detected in suspended biomass and anammox granules in Phase 2B. Previous studies have shown that the *amoA* gene is associated with the sulfammox process, in which $NH_4^+$ could be oxidized to $NO_2^-$ for anammox (Zhang et al., 2025).

In the $S^0$PDA process, sulfur metabolism is accompanied by nitrogen metabolism, and S-related genes are shown in Fig. 6B. The *soxAXY* genes, which are involved in the oxidation of $S^0$ to $SO_4^{2-}$, were associated with *Thiobacillus*; the *soxAXY* genes decreased in the suspend biomass from Phase 1A to Phase 2B. This might have been due to the decrease of SOB's abundance. As shown in Fig. 6C, $SO_4^{2-}$ reduction was mediated by a group of genes primarily associated with *Thiobacillus*, including the *sat* gene (encoding sulfate adenylyltransferase) and the *aprAB* gene (encoding adenylylsulfate reductase). These genes also were detected in anammox granules and related to *Candidatus Brocadia*, perhaps suggesting its involvement in the sulfammox process in cooperation with *Thiobacillus*. This finding aligns with previous studies showing that *Candidatus Brocadia* mediating nitrification and $SO_4^{2-}$ reduction in sulfammox process (Jiang et al., 2025; Zhang et al., 2025).

Overall, anammox bacteria (*Candidatus Brocadia*) and SOB (*Thiobacillus*) jointly established a N—S cycle to enhance nitrogen-removal; this relationship is illustrated in Fig. S5. In the $S^0$D process, $S^0$ powders and the reduced sulfur compounds produced from sulfammox were oxidized to reduce $NO_3^-$, which was from influent and anammox process, to $NO_2^-$. In the sulfammox process, $SO_4^{2-}$ produced from $S^0$ oxidization could serve as an electron acceptor to oxidize $NH_4^+$ to $NO_2^-$. Finally, the $NO_2^-$ from $S^0$D and sulfammox was utilized via anammox. $S^0$ powders supported this cooperative mechanism and facilitated electron transfer and substrate exchange.

## 4. Conclusions

This study evaluated a novel $S^0$PD/A process that, by integrating anammox granules with $S^0$ powders, achieved good nitrogen-removal performance without addition of organic electron donors. A stable synergy was established between SOB and anammox bacteria, which inhabited different spatial *niches*: *Thiobacillus* (SOB) formed microgranules in the suspended solids colonizing the $S^0$ powders, while *Candidatus Brocadia* (anammox bacteria) was predominantly localized within the anammox granules. This spatial organization promoted effective substrate exchange and electron transfer that established among $S^0$D, anammox, and sulfammox.

## CRediT authorship contribution statement

**Sen Wang:** Writing – original draft, Methodology, Data curation, Conceptualization. **Ben Dai:** Visualization, Writing – review & editing. **Zhenyu Wang:** Visualization, Investigation. **Shaobo Yang:** Visualization, Investigation. **Siqing Xia:** Supervision, Project administration, Funding acquisition. **Bruce E. Rittmann:** Writing – review & editing, Visualization.

## Declaration of competing interest

The authors declare that they have no known competing financial interests or personal relationships that could have appeared to influence the work reported in this paper.

## Acknowledgements

This work was supported by National Key Project of Research and Development Plan of China (2021YFC3201300). The authors would like to acknowledge Prof. Bruce E. Rittmann for his help with the review, editing, and visualization of the manuscript.

## Appendix A. Supplementary data

Supplementary data to this article can be found online at https://doi.org/10.1016/j.biortech.2025.133707.

## Data availability

Data will be made available on request.

## References

APHA, 1998. Standard Methods for the Examination of Water and Wastewater. American Public Health Association, Washington, DC, USA.
Campo, R., Corsino, S.F., Torregrossa, M., Di Bella, G., 2018. The role of extracellular polymeric substances on aerobic granulation with stepwise increase of salinity. Sep. Purif. Technol. 195, 12–20.
Cao, S., Rui, D., Zhou, Y., 2021. Coupling anammox with heterotrophic denitrification for enhanced nitrogen removal: a review. Crit. Rev. Environ. Sci. Technol. 51 (19), 2260–2293.
Chen, F., Li, X., Gu, C., Huang, Y., Yuan, Y., 2018. Selectivity control of nitrite and nitrate with the reaction of S0 and achieved nitrite accumulation in the sulfur autotrophic denitrification process. Bioresour. Technol. 266, 211–219.
Deng, Y.-F., Ekama, G.A., Cui, Y.-X., Tang, C.-J., van Loosdrecht, M.C., Chen, G.-H., Wu, D., 2019a. Coupling of sulfur (thiosulfate)-driven denitratation and anammox process to treat nitrate and ammonium contained wastewater. Water Res. 163, 114854.
Deng, Y.-F., Ekama, G.A., Cui, Y.-X., Tang, C.-J., van Loosdrecht, M.C.M., Chen, G.-H., Wu, D., 2019b. Coupling of sulfur(thiosulfate)-driven denitratation and anammox process to treat nitrate and ammonium contained wastewater. Water Res. 163, 114854.
Deng, Y.-F., Zan, F.-X., Huang, H., Wu, D., Tang, W.-T., Chen, G.-H., 2022. Coupling sulfur-based denitrification with anammox for effective and stable nitrogen removal: a review. Water Res. 224, 119051.
Du, R., Cao, S., Zhang, H., Li, X., Peng, Y., 2020. Flexible nitrite supply alternative for mainstream anammox: advances in enhancing process stability. Environ. Sci. Technol. 54 (10), 6353–6364.
Du, Z., Wang, J., Zhang, F., Peng, Y., 2024. Autotrophic sulfur-driven partial denitrification as a sustainable nitrite supply pathway for anammox: insights on enhanced nitrogen removal and microbial synergies. ACS ES&T Water.
Gu, Z., Liu, Z., Cheng, Y., Zhu, Z., Tian, J., Hu, C., Qu, J., 2024. Intensified denitrification in a fluidized-bed reactor with suspended sulfur autotrophic microbial fillers. Bioresour. Technol. 391, 129965.
Hu, Y., Wu, G., Li, R., Xiao, L., Zhan, X., 2020. Iron sulphides mediated autotrophic denitrification: an emerging bioprocess for nitrate pollution mitigation and sustainable wastewater treatment. Water Res. 179, 115914.
Jiang, Z., He, Y., Zeng, M., Cao, S., Liu, W., Liu, L., Wang, S., 2025. Unraveling the mechanisms of anammox coupled process with thiosulfate-driven denitrification: Community succession and substrate competition. Environ. Res. 264, 120372.
Jimenez, J., Miller, M., Bott, C., Murthy, S., De Clippeleir, H., Wett, B., 2015. High-rate activated sludge system for carbon management - evaluation of crucial process mechanisms and design parameters. Water Res. 87, 476–482.
Kosgey, K., Chandran, K., Gokal, J., Kiambi, S.L., Bux, F., Kumari, S., 2021. Critical analysis of biomass retention strategies in mainstream and sidestream ANAMMOX-mediated nitrogen removal systems. Environ. Sci. Technol. 55 (1), 9–24.
Li, Y., Chen, B., Zhang, X., Luo, Z., Lei, M., Song, T., Long, Z., Li, J., Ma, J., 2023. Elemental sulfur autotrophic partial denitrification (S0-PDN) with high pH and free ammonia control strategy for low-carbon wastewater: from performance to microbial mechanism. Chem. Eng. J. 474, 145419.
Liang, Z., Yi, J., Cao, D., Shi, J., Yang, D., Dai, L., Dai, X., 2022. High concentration powder carrier bio-fluidized bed process: a new perspective for domestic wastewater treatment. Bioresour. Technol. 351.
Liu, Y., Deng, Y., van Loosdrecht, M.C.M., Chen, G., 2025. Development of nitrification and elemental sulfur-based denitrification/anammox (NS0DA) process for mainstream nitrogen removal. Water Res. 123836.
Lotti, T., Kleerebezem, R., Abelleira-Pereira, J.M., Abbas, B., van Loosdrecht, M.C.M., 2015. Faster through training: the anammox case. Water Res. 81, 261–268.
Lu, D., Gong, H., Diao, S., Shi, W., Yin, R., Dai, X., 2023. Enhanced sludge settlement of two stage PN/Anammox for reject water treatment with respective diatomite addition. Sci. Total Environ. 877, 162784.
Qian, J., Bai, L., Zhang, M., Chen, L., Yan, X., Sun, R., Zhang, M., Chen, G.-H., Wu, D., 2021. Achieving rapid thiosulfate-driven denitrification (TDD) in a granular sludge system. Water Res. 190, 116716.
Strous, M., Kuenen, J.G., Jetten Mike, S.M., 1999. Key physiology of anaerobic ammonium oxidation. Appl. Environ. Microbiol. 65 (7), 3248–3250.

Wang, H., Xu, H., Liu, X., Hua, Y., Yang, D., Dai, X., 2024a. A novel process based on powder carriers demonstrates robustness in nitrogen and phosphorus removal from real municipal wastewater. Water Res. 251.
Wang, H., Yu, G., He, W., Du, C., Deng, Z., Wang, D., Yang, M., Yang, E., Zhou, Y., Sanjaya, E.H., Chen, H., 2021. Enhancing autotrophic nitrogen removal with a novel dissolved oxygen-differentiated airlift internal circulation reactor: long-term operational performance and microbial characteristics. J. Environ. Manage. 296, 113271.
Wang, L., Zhao, Q., Zhang, L., Wu, D., Zhou, J., Peng, Y., 2024b. S0-driven partial denitrification coupled with anammox (S0PDA) enables highly efficient autotrophic nitrogen removal from wastewater. Water Res. 255.
Wang, S., Liu, L., Li, H., Fang, F., Yan, P., Chen, Y., Guo, J., Ma, T., Shen, Y., 2020. The branched chains and branching degree of exopolysaccharides affecting the stability of anammox granular sludge. Water Res. 178, 115818.
Wang, T., Li, X., Wang, H., Xue, G., Zhou, M., Ran, X., Wang, Y., 2023. Sulfur autotrophic denitrification as an efficient nitrogen removals method for wastewater treatment towards lower organic requirement: a review. Water Res. 245, 120569.
Wang, X., Yang, H., Su, Y., Liu, X., 2022. Effects of sludge morphology on the anammox process: Analysis from the perspectives of performance, structure, and microbial community. Chemosphere 288, 132390.
Wu, B., Wang, X., Wang, C., Lu, B., Yi, J., Dai, X., Chai, X., 2022. Novel micro-granular sludge process for highly efficient treatment of low-strength and low C/N ratio municipal wastewater. Chemosphere 287, 132322.
Xue, Y., Ma, H., Li, Y.-Y., 2023. Anammox-based granulation cycle for sustainable granular sludge biotechnology from mechanisms to strategies: a critical review. Water Res. 228, 119353.
Yin, C., Meng, F., Chen, G.-H., 2015. Spectroscopic characterization of extracellular polymeric substances from a mixed culture dominated by ammonia-oxidizing bacteria. Water Res. 68, 740–749.
Yin, S., Wang, Y.-X., Hou, C., Wang, J., Xu, J., Jiang, X., Chen, D., Mu, Y., Shen, J., 2025. Deciphering the key role of biofilm and mechanisms in high-strength nitrogen removal within the anammox coupled partial S0-driven autotrophic denitrification system. Bioresour. Technol. 419, 132020.
Yu, J., Xiao, K., Xu, H., Li, Y., Xue, Q., Xue, W., Zhang, A., Wen, X., Xu, G., Huang, X., 2023. Spectroscopic fingerprints profiling the polysaccharide/protein/humic architecture of stratified extracellular polymeric substances (EPS) in activated sludge. Water Res. 235, 119866.
Zeng, C., Su, Q., Peng, L., Sun, L., Zhao, Q., Diao, X., Lu, H., 2021. Elemental sulfur-driven autotrophic denitrification for advanced nitrogen removal from mature landfill leachate after PN/A pretreatment. Chem. Eng. J. 410, 128256.
Zhang, F., Peng, Y., Liu, Y., Zhao, L., 2021. Improving stability of mainstream Anammox in an innovative two-stage process for advanced nitrogen removal from mature landfill leachate. Bioresour. Technol. 340, 125617.
Zhang, J., Peng, Y., Li, X., Du, R., 2022. Feasibility of partial-denitrification/ anammox for pharmaceutical wastewater treatment in a hybrid biofilm reactor. Water Res. 208, 117856.
Zhang, M., Wang, S., Ji, B., Liu, Y., 2019. Towards mainstream deammonification of municipal wastewater: Partial nitrification-anammox versus partial denitrification-anammox. Sci. Total Environ. 692, 393–401.
Zhang, Z., Zhang, C., Yang, Y., Zhang, Z., Guo, K., Zhang, X., Qin, Z., Huang, J., Li, Y., 2025. Roles of nitrite in facilitating nitrogen and sulfur conversion in the hybrid bioreactor of Sulfate-reduced ammonium oxidation and anaerobic ammonium oxidation. Bioresour. Technol. 419, 132085.
Zhen, J., Wang, Z.-B., Ni, B.-J., Ismail, S., El-Baz, A., Cui, Z., Ni, S.-Q., 2024. Synergistic integration of anammox and endogenous denitrification processes for the simultaneous carbon, nitrogen, and phosphorus removal. Environ. Sci. Technol. 58 (24), 10632–10643.
Zhou, W., Sun, Y., Wu, B., Zhang, Y., Huang, M., Miyanaga, T., Zhang, Z., 2011. Autotrophic denitrification for nitrate and nitrite removal using sulfur-limestone. J. Environ. Sci. 23 (11), 1761–1769.
Zhu, Z., Qin, J., Chen, Z., Chen, Y., Chen, H., Wang, X., 2022. Sulfammox forwarding thiosulfate-driven denitrification and anammox process for nitrogen removal. Environ. Res. 214, 113904.